THE EUROPEAN
PHYSICAL JOURNAL C

CrossMark

Regular Article - Theoretical Physics

On the possibility to detect the Higgs decay $H \to b\bar{b}$ in the associated $Z + b\bar{b}$ production at the LHC

A. V. Lipatov[1,2,a], **N. P. Zotov**[1]

[1] Skobeltsyn Institute of Nuclear Physics, Lomonosov Moscow State University, 119991 Moscow, Russia
[2] Joint Institute for Nuclear Research, 141980 Dubna, Moscow Region, Russia

Abstract We investigate the possibility to detect the scalar Higgs boson decay $H \to b\bar{b}$ in the associated Z and $b\bar{b}$ production at the LHC using the k_T-factorization QCD approach. Our consideration is based on the off-shell (i.e. depending on the transverse momenta of initial quarks and gluons) production amplitudes of $q^*\bar{q}^* \to ZH \to Zq'\bar{q}'$, $q^*\bar{q}^* \to Zq'\bar{q}'$, and $g^*g^* \to Zq'\bar{q}'$ partonic subprocesses supplemented with the Catani–Ciafoloni–Fiorani–Marchesini (CCFM) dynamics of parton densities in a proton. We argue that the $H \to b\bar{b}$ signal could be observed at large transverse momenta near the Higgs boson peak despite the overwhelming QCD background, and we point out the important role of angular correlations between the produced Z boson and b-quarks.

In 2012, during the search performed by the CMS and ATLAS Collaborations at the LHC, the scalar Higgs boson H with a mass m_H near 125 GeV has been discovered [1,2], giving us the confidence in the physical picture of fundamental interactions which follows from the Standard Model Lagrangian. Some time later, the ATLAS Collaboration has reported first measurements of the Higgs boson differential cross sections in the $\gamma\gamma$ decay mode [3]. The measured cross sections were found to be a bit higher than the central next-to-next-to-leading order (NNLO) expectations [4–9] and those matched with a soft-gluon resummation carried out up to next-to-next-to-leading logarithmic accuracy (NNLL) [10,11], although no significant deviations from the theoretical predictions are observed within the uncertainties [3]. The significant signal was detected also in channels where the Higgs boson decays into the ZZ or WW pairs [12,13]. The interaction of the Higgs particle with the massive Z and W bosons indicates that, as expected, it plays a role in electroweak symmetry breaking. However,

the interaction with the fermions and whether the Higgs field serves as the source of mass generation in the fermion sector still remain to be established. Since the Higgs boson with mass $m_H \sim 125$ GeV decays mainly into a beauty quark–antiquark pair [14], the observation and study of the $H \to b\bar{b}$ decay (which involves the direct coupling of the Higgs boson to beauty quarks) is therefore essential in determining the nature of the newly discovered boson.

The most sensitive channel for the $H \to b\bar{b}$ events at the LHC is the production of a Higgs particle in association with the Z boson [15]. Despite the largest branching fraction ($\sim 58\,\%$), the $H \to b\bar{b}$ final state is more difficult for the experimental observation compared to the signatures provided by the diphoton or diboson decay modes due to the small signal over background ratio. One of the main backgrounds for the associated Higgs and Z boson production is the associated production of Z boson and two b-quark jets. The corresponding cross sections, calculated at the NNLO level (see [14]), are several orders of magnitude larger than the Higgs boson signal. However, recently the CMS Collaboration reported [16] an excess of events above the expected background with a local significance of 2.1 standard deviations, which is compatible with a Higgs boson mass of 125 GeV. Earlier, the CDF and D0 Collaborations at the Tevatron also reported [15] evidence for an excess of events in the 115–140 GeV mass range, consistent with the mass of the Higgs boson observed at the LHC.

The experimental searches [15,16] have stimulated us to investigate the associated Higgs (decaying into a $b\bar{b}$ pair) and Z boson production as well as the corresponding main background process, the associated production of Z boson and two b-quark jets,[1] using the k_T-factorization approach of QCD [17–20]. A detailed description of this formalism can be found, for example, in the reviews in Refs. [21–23].

---

[1] Other background processes, like the $t\bar{t}$ pair, diboson or QCD multijet production are beyond our present consideration.

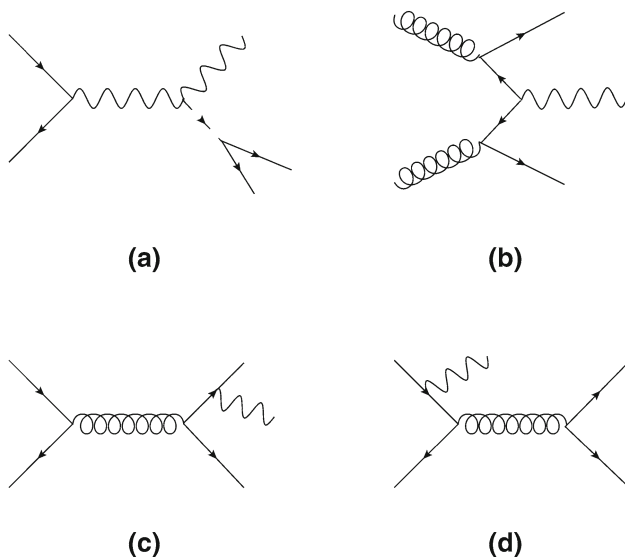**Fig. 1** Examples of Feynman diagrams corresponding to $q^*\bar{q}^* \to ZH \to Zb\bar{b}$ (**a**), $g^*g^* \to Zb\bar{b}$ (**b**) and $q^*\bar{q}^* \to Zb\bar{b}$ (**c**, **d**) subprocesses. The full set of diagrams can be obtained by permutations of the quark, gluon, Higgs, and Z boson lines

We only mention that the main part of the higher-order QCD corrections (namely, NLO + NNLO + N³LO + ··· contributions, which correspond to the log $1/x$ enhanced terms in perturbative series) is effectively taken into account in the k_T-factorization approach already at leading order, and it provides a solid theoretical ground for the effects of the initial parton radiation and transverse momenta of the initial quarks and gluons. Recently, the k_T-factorization QCD approach was successfully applied [24,25] to describe the ATLAS data [3] on the inclusive Higgs production in the diphoton decay mode.[2]

Let us start from a short review of the steps of the calculation. Our consideration is based on the off-shell (depending on the transverse momenta of initial partons) partonic subprocesses:

$$q^*(k_1) + \bar{q}^*(k_2) \to Z + H \to Z(p) + q'(p_1) + \bar{q}'(p_2),$$
$$\tag{1}$$

$$q^*(k_1) + \bar{q}^*(k_2) \to Z(p) + q'(p_1) + \bar{q}'(p_2), \tag{2}$$

$$g^*(k_1) + g^*(k_2) \to Z(p) + q'(p_1) + \bar{q}'(p_2), \tag{3}$$

where the four-momenta of all corresponding particles are given in the parentheses (see Fig. 1). The subprocesses (2) and (3) correspond to the main QCD background to the associated Higgs and Z boson production. Note that, to calculate the production amplitudes, we apply the reggeized parton approach [26,27], which is based on the effective action formalism [28,29], currently explored at next-to-leading order

---

[30–32], and we take into account the virtualities of both initial quarks and gluons. In this point our consideration differs from the one based on the collinear QCD factorization, where these virtualities are not taken into account. The use of effective vertices [26,27] ensures the exact gauge invariance of the calculated amplitudes despite the off-shell initial partons.

The off-shell amplitude of the subprocess (1) reads

$$\mathcal{M}_1 = ee_q\, \epsilon^\mu(p)\, \bar{v}_{s_1}(p_2)\Gamma_{Hq\bar{q}}u_{s_2}(p_1)$$
$$\times \frac{1}{(p_1+p_2)^2 - m_H^2 - im_H\Gamma_H}$$
$$\times \Gamma_{ZZH}^{\mu\nu}\left[g^{\nu\lambda} - \frac{(k_1+k_2)^\nu(k_1+k_2)^\lambda}{m_Z^2}\right]$$
$$\times \frac{1}{\hat{s} - m_Z^2 - im_Z\Gamma_Z}\,\bar{v}_{r_1}(x_2l_2)\Gamma_{q^*\bar{q}^*Z}^\lambda u_{r_2}(x_1l_1), \tag{4}$$

where e and e_q are the electron and incoming quark (fractional) electric charges, ϵ^μ is the polarization 4-vector of produced Z boson, $\hat{s} = (k_1+k_2)^2$, $k_i = x_il_i + k_{iT}$ (with $i = 1$ or 2), l_1 and l_2 are the 4-momenta of colliding protons, x_1 and x_2 are the corresponding momentum fractions and Γ_H is the full decay width of the Higgs boson, m_Z and Γ_Z are the mass and full decay width of the Z boson. We will take the propagators of intermediate Z and Higgs bosons in the Breit–Wigner form to avoid any artificial singularities in the numerical calculations. The fermion and gauge boson to Higgs vertices are the usual

$$\Gamma_{Hq\bar{q}} = -\frac{e}{\sin 2\theta_W}\frac{m_{q'}}{m_Z}, \tag{5}$$

$$\Gamma_{ZZH}^{\mu\nu} = \frac{e}{\sin 2\theta_W}g^{\mu\nu}m_Z, \tag{6}$$

where $m_{q'}$ is the mass of the produced quark or antiquark, and θ_W is the Weinberg mixing angle. We will neglect the masses of the initial quarks compared to the masses of final state particles but keep their non-zero transverse momenta: $\mathbf{k}_{1T}^2 = -k_{1T}^2 \neq 0$, $\mathbf{k}_{2T}^2 = -k_{2T}^2 \neq 0$. The effective vertex $\Gamma_{q^*\bar{q}^*Z}^\mu$, which describes the effective coupling of an off-shell quark and antiquark to the Z boson, reads [26,27] (see also [33])

$$\Gamma_{q^*\bar{q}^*Z}^\mu = \left[\gamma^\mu - \hat{k}_1\frac{l_1^\mu}{(l_1\cdot k_2)} - \hat{k}_2\frac{l_2^\mu}{(l_2\cdot k_1)}\right]\left(C_V^q - C_A^q\gamma^5\right), \tag{7}$$

where C_V^q and C_A^q are the corresponding vector and axial coupling constants. The effective vertex $\Gamma_{q^*\bar{q}^*Z}^\mu$ satisfies the Ward identity $\Gamma_{q^*\bar{q}^*Z}^\mu(k_1+k_2)_\mu = 0$. The off-shell amplitude of the subprocess (2) reads

$$\mathcal{M}_2 = ee_{q'}g^2t^a\delta^{ab}t^b\epsilon^\mu(p)\,\bar{v}_{s_1}(p_2)F_1^{\mu\nu}u_{s_2}(p_1)$$
$$\times \frac{g^{\nu\lambda}}{(k_1+k_2)^2}\,\bar{v}_{r_1}(x_2l_2)\Gamma_{q^*\bar{q}^*g}^\lambda u_{r_2}(x_1l_1)$$

$$+ e e_q g^2 t^a \delta^{ab} t^b \epsilon^\mu(p) \, \bar{v}_{s_1}(p_2) F_2^{\mu\lambda} u_{s_2}(p_1)$$

$$\times \frac{g^{\nu\lambda}}{(p_1 + k_2)^2} \bar{v}_{r_1}(x_2 l_2) \gamma^\nu u_{r_2}(x_1 l_1), \tag{8}$$

where $e_{q'}$ is the produced quark (fractional) electric charge, g is the strong charge, a and b are the eight-fold color indices, and

$$F_1^{\mu\nu} = \Gamma_{qqZ}^\mu \frac{\hat{p} + \hat{p}_1 + m_{q'}}{(p + p_1)^2 - m_{q'}^2} \gamma^\nu$$

$$+ \gamma^\nu \frac{-\hat{p} - \hat{p}_2 + m_{q'}}{(-p - p_2)^2 - m_{q'}^2} \Gamma_{qqZ}^\mu, \tag{9}$$

$$F_2^{\mu\lambda} = \Gamma_{q^*qg}^{(+)\lambda}(k_2, p_1 + p_2) \frac{\hat{k}_1 - \hat{p}}{(k_1 - p)^2} \Gamma_{q^*qZ}^{(-)\mu}(k_1, p)$$

$$+ \Gamma_{q^*qZ}^{(+)\mu}(k_2, p) \frac{-\hat{k}_2 - \hat{p}}{(-k_2 - p)^2} \Gamma_{q^*qg}^{(-)\lambda}(k_1, p_1 + p_2)$$

$$+ \Delta^{\mu\lambda}(k_1, -k_2, p, p_1 + p_2). \tag{10}$$

The on-shell quark coupling to the Z boson is taken in a standard form:

$$\Gamma_{qqZ}^\mu = \gamma^\mu \left(C_V^q - C_A^q \gamma^5 \right). \tag{11}$$

The effective vertices can be written as [26,27]

$$\Gamma_{q^*\bar{q}^*g}^\mu = \gamma^\mu - \hat{k}_1 \frac{l_1^\mu}{(l_1 \cdot k_2)} - \hat{k}_2 \frac{l_2^\mu}{(l_2 \cdot k_1)}, \tag{12}$$

$$\Gamma_{q^*qg}^{(+)\mu}(k, q) = \gamma^\mu - \hat{k} \frac{l_1^\mu}{(l_1 \cdot q)}, \tag{13}$$

$$\Gamma_{q^*qg}^{(-)\mu}(k, q) = \gamma^\mu - \hat{k} \frac{l_2^\mu}{(l_2 \cdot q)}. \tag{14}$$

The corresponding couplings of the off-shell quark or anti-quark to the usual on-shell quark and Z boson are constructed as was done earlier [33]:

$$\Gamma_{q^*qZ}^{(\pm)\mu}(k, q) = \Gamma_{q^*qg}^{(\pm)\mu}(k, q)(C_V^q - C_A^q \gamma^5). \tag{15}$$

The induced term $\Delta^{\mu\nu}(k_1, k_2, q_1, q_2)$ has the form [34]

$$\Delta^{\mu\nu}(k_1, k_2, q_1, q_2) = \hat{k}_1 \frac{l_1^\mu l_1^\nu}{(q_1 \cdot l_1)(q_2 \cdot l_1)}$$

$$+ \hat{k}_2 \frac{l_2^\mu l_2^\nu}{(q_1 \cdot l_2)(q_2 \cdot l_2)}. \tag{16}$$

The summation on the produced Z boson polarizations is carried out with the usual covariant formula:

$$\sum \epsilon^\mu(p) \epsilon^{*\nu}(p) = -g^{\mu\nu} + \frac{p^\mu p^\nu}{m_Z^2}. \tag{17}$$

In according to the k_T-factorization prescription [17–20], the summation over the polarizations of the incoming off-shell gluons is carried out with $\sum \epsilon^\mu \epsilon^{*\nu} = \mathbf{k}_T^\mu \mathbf{k}_T^\nu / \mathbf{k}_T^2$. In the collinear limit, when $|\mathbf{k}_T| \to 0$, this expression converges to the ordinary one after averaging on the azimuthal angle. According to the use of the effective vertices, the spin density matrix for off-shell spinors in the initial state is taken in the usual form $\sum u(x_i l_i) \bar{u}(x_i l_i) = x_i \hat{l}_i + m$ (where $i = 1$ or 2, and we omitted the spinor indices). Further calculations are straightforward and in other respects follow the standard QCD Feynman rules. The evaluation of the traces was performed using the algebraic manipulation system FORM [35]. We do not list here the obtained lengthy expressions because of lack of space. The off-shell amplitude of the gluon–gluon fusion subprocess (3) was derived in our previous paper [36] (see also [37]).

The cross section of any process in the k_T-factorization approach is calculated as a convolution of the off-shell partonic cross section and the unintegrated, or transverse momentum dependent (TMD), parton densities in a proton. The cross sections of the subprocesses (1) and (2) read

$$\sigma = \sum_q \int \frac{1}{256\pi^3 (x_1 x_2 s)^2} |\bar{\mathcal{M}}_{1,2}|^2$$

$$\times f_q(x_1, \mathbf{k}_{1T}^2, \mu^2) f_q(x_2, \mathbf{k}_{2T}^2, \mu^2)$$

$$\times d\mathbf{k}_{1T}^2 d\mathbf{k}_{2T}^2 \mathbf{p}_{1T}^2 \mathbf{p}_{2T}^2 dy dy_1 dy_2$$

$$\times \frac{d\phi_1}{2\pi} \frac{d\phi_2}{2\pi} \frac{d\psi_1}{2\pi} \frac{d\psi_2}{2\pi}, \tag{18}$$

where $f_q(x_i, \mathbf{k}_{iT}^2, \mu^2)$ is the TMD quark density in a proton, y is the rapidity of the produced Z boson, s is the total energy, $\mathbf{p}_{1T}$, $\mathbf{p}_{2T}$, y_1, y_2, ψ_1, and ψ_2 are the transverse momenta, rapidities, and azimuthal angles of the final state quarks, respectively. The incoming quarks have azimuthal angles ϕ_1 and ϕ_2. The cross sections of the subprocess (3) can be written as

$$\sigma = \int \frac{1}{256\pi^3 (x_1 x_2 s)^2} |\bar{\mathcal{M}}_3|^2$$

$$\times f_g(x_1, \mathbf{k}_{1T}^2, \mu^2) f_g(x_2, \mathbf{k}_{2T}^2, \mu^2) d\mathbf{k}_{1T}^2 d\mathbf{k}_{2T}^2$$

$$\times d\mathbf{p}_{1T}^2 \mathbf{p}_{2T}^2 dy dy_1 dy_2$$

$$\times \frac{d\phi_1}{2\pi} \frac{d\phi_2}{2\pi} \frac{d\psi_1}{2\pi} \frac{d\psi_2}{2\pi}, \tag{19}$$

where $f_g(x_i, \mathbf{k}_{iT}^2, \mu^2)$ is the TMD gluon density in a proton, and $\mathcal{M}_3$ is the off-shell amplitude of the subprocess (3).

Concerning the TMD parton densities in a proton, we concentrate on the approach based on the CCFM evolution equation [38–41]. The CCFM parton shower, based on the principle of color coherence, describes only the emission of gluons, while real quark emissions are left aside. It implies that the CCFM equation describes only the distinct evolution of
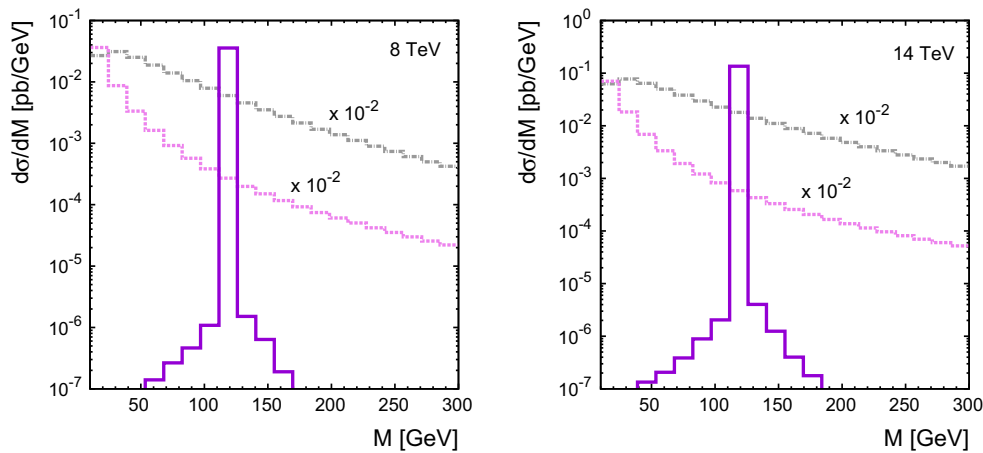
Fig. 2 The associated $Z + b\bar{b}$ cross sections in pp collisions calculated as a function of invariant mass of $b\bar{b}$ quarks at $\sqrt{s} = 8$ TeV (*left panel*) and $\sqrt{s} = 14$ TeV (*right panel*). The *solid*, *dashed* and *dash-dotted histograms* correspond to the contributions from the $q^*\bar{q}^* \to ZH \to Zb\bar{b}$, $q^*\bar{q}^* \to Zb\bar{b}$, and $g^*g^* \to Zb\bar{b}$ subprocesses, respectively. No cuts are applied

TMD gluon and valence quarks, while the non-diagonal transitions between quarks and gluons are absent. Below we use the TMD gluon and valence quark distributions which were obtained [42,43] from the numerical solutions of the CCFM equation (namely, set A0). Following [44], we calculate the TMD sea quark density with the approximation where the sea quarks occur in the last gluon-to-quark splitting. At the next-to-leading logarithmic accuracy $\alpha_s(\alpha_s \ln x)^n$, the TMD sea quark distribution can be written as follows [44]:

$$f_q^{(\text{sea})}(x, \mathbf{k}_T^2, \mu^2) = \int_x^1 \frac{dz}{z} \int d\mathbf{q}_T^2 \frac{1}{\Delta^2} \frac{\alpha_s}{2\pi}$$
$$\times P_{qg}(z, \mathbf{q}_T^2, \Delta^2) f_g(x/z, \mathbf{q}_T^2, \bar{\mu}^2), \tag{20}$$

where z is the fraction of the gluon light cone momentum carried out by the quark, and $\Delta = \mathbf{k}_T - z\mathbf{q}_T$. The sea quark evolution is driven by the off-shell gluon-to-quark splitting function $P_{qg}(z, \mathbf{q}_T^2, \Delta^2)$ [45,46]:

$$P_{qg}(z, \mathbf{q}_T^2, \Delta^2) = T_R \left(\frac{\Delta^2}{\Delta^2 + z(1-z)\,\mathbf{q}_T^2} \right)^2$$
$$\times \left[(1-z)^2 + z^2 + 4z^2(1-z)^2 \frac{\mathbf{q}_T^2}{\Delta^2} \right], \tag{21}$$

where $T_R = 1/2$. The splitting function $P_{qg}(z, \mathbf{q}_T^2, \Delta^2)$ has been obtained by generalizing to finite transverse momenta, in the high-energy region, the two-particle irreducible kernel expansion [47]. It takes into account the small-x enhanced transverse momentum dependence up to all orders in the strong coupling constant, and it reduces to the conventional

splitting function at lowest order for $|\mathbf{q}_T| \to 0$. The scale $\bar{\mu}^2$ is defined [48] from the angular ordering condition, which is natural from the point of view of the CCFM evolution: $\bar{\mu}^2 = \Delta^2/(1-z)^2 + \mathbf{q}_T^2/(1-z)$.

Other essential parameters were taken as follows: renormalization scale $\mu_R^2 = m_Z^2 + p_T^2$, factorization scale $\mu_F^2 = \hat{s} + \mathbf{Q}_T^2$ (with $\mathbf{Q}_T$ being the transverse momentum of initial parton pair), beauty quark mass $m_b = 4.75$ GeV, $m_Z = 91.1876$ GeV, $m_H = 125$ GeV, $\Gamma_Z = 2.4952$ GeV, $\Gamma_H = 4.3$ MeV, $\sin^2 \theta_W = 0.23122$, and we use the LO formula for the strong coupling constant $\alpha_s(\mu^2)$ with $n_f = 4$ active quark flavors at $\Lambda_{\text{QCD}} = 200$ MeV, so that $\alpha_s(m_Z^2) = 0.1232$. To take into account the non-logarithmic loop corrections to the production cross sections, we apply the effective K-factor, as was done in [49–51]:

$$K = \exp\left[C_F \frac{\alpha_s(\mu^2)}{2\pi} \pi^2 \right], \tag{22}$$

where the color factor $C_F = 4/3$. A particular choice of the scale, $\mu^2 = p_T^{4/3} m_Z^{2/3}$, was proposed [49–51] to eliminate sub-leading logarithmic terms. Note that we choose this scale to evaluate the strong coupling constant in (22) only. Everywhere the multidimensional integration has been performed by means of the Monte Carlo technique, using the routine VEGAS [52]. The corresponding C++ code is available from the authors on request.

We now are in a position to present our numerical predictions. The differential cross sections of the associated $Zb\bar{b}$ production in pp collisions as a function of M, the invariant mass of the final beauty quarks, and Z boson transverse momentum at $\sqrt{s} = 8$ and 14 TeV are shown in Figs. 2 and 3. The solid, dashed, and dash-dotted histograms correspond to the contributions from the subprocesses (1), (2), and (3),
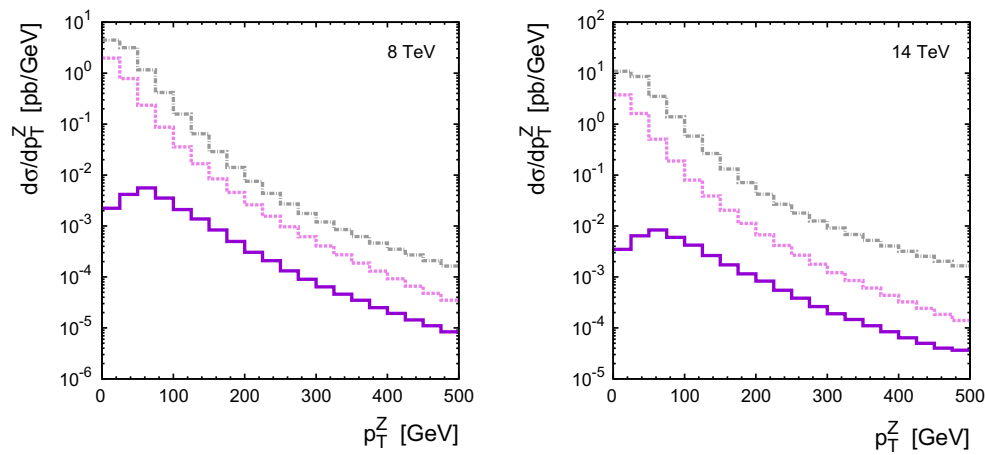
Fig. 3 The associated $Z + b\bar{b}$ cross sections in pp collisions calculated as a function of Z boson transverse momentum at $\sqrt{s} = 8$ TeV (*left panel*) and $\sqrt{s} = 14$ TeV (*right panel*). The notation of all histograms is the same as in Fig. 2. No cuts are applied
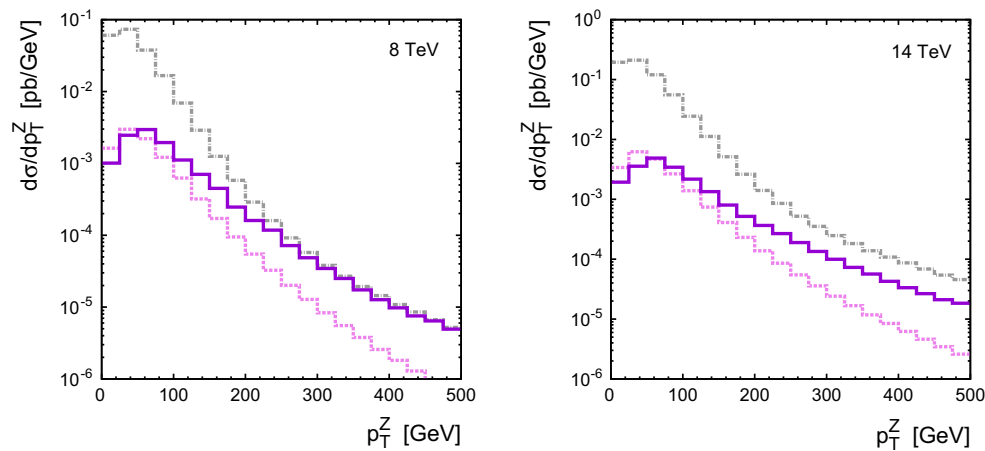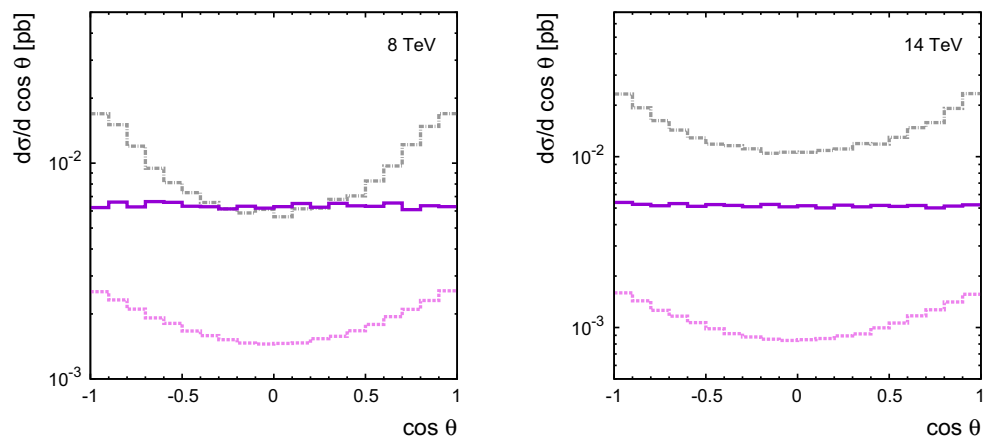

Fig. 4 The associated $Z + b\bar{b}$ cross sections in pp collisions calculated as a function of Z boson transverse momentum at $\sqrt{s} = 8$ TeV (*left panel*) and $\sqrt{s} = 14$ TeV (*right panel*) at $120 < M < 130$ GeV. The notation of all histograms is the same as in Fig. 2

Fig. 5 The associated $Z + b\bar{b}$ cross sections in pp collisions calculated as a function of angle θ between the produced Z boson and beauty quark in the Collins–Soper frame at $\sqrt{s} = 8$ TeV (*left panel*) and $\sqrt{s} = 14$ TeV (*right panel*) at $120 < M < 130$ GeV. An additional cut $p_T > 200(300)$ GeV is applied for $\sqrt{s} = 8(14)$ TeV. The notation of all histograms is the same as in Fig. 2
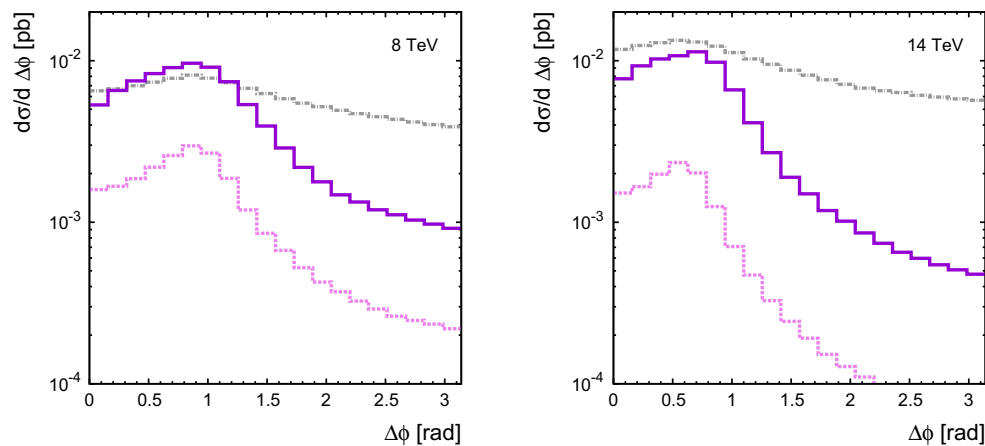
Fig. 6 The associated $Z+b\bar{b}$ cross sections in pp collisions calculated as a function of azimuthal angle difference $\Delta\phi$ between the produced beauty quarks in the pp center-of-mass frame at $\sqrt{s} = 8$ TeV (*left panel*) and $\sqrt{s} = 14$ TeV (*right panel*) at $120 < M < 130$ GeV. An additional cut $p_T > 200(300)$ GeV is applied for $\sqrt{s} = 8(14)$ TeV. The notation of all histograms is the same as in Fig. 2

respectively. There are no cuts applied at all. One can see that the associated Higgs (decaying into the $b\bar{b}$ pair) and Z boson production cross section lies below the QCD backgrounds by several orders of magnitude in the whole p_T range, but it peaks near the Higgs mass. To increase the relative contribution from the Higgs signal, we repeated the calculations in the restricted region of M, namely $120 < M < 130$ GeV (see Fig. 4). We found that here the associated Higgs and Z boson production gives a sizeable contribution to the $Zb\bar{b}$ cross section at high Z boson transverse momenta. So, at $\sqrt{s} = 8$ TeV it practically coincides with the leading contribution from the gluon–gluon fusion subprocess at $p_T > 200$ GeV. At $\sqrt{s} = 14$ TeV, it lies below this value. However, these contributions are almost comparable at $p_T > 300$ GeV. With the expected LHC luminosity of about 40 fb^{-1}, our estimation gives 400–500 events (with beauty quarks originating from the Higgs boson decays) for both energies, 8 and 14 TeV. Therefore, the possibility for the experimental detection of the Higgs signal appears in the kinematical region defined above.

A special opportunity to detect the decays of scalar Higgs bosons can be provided by the investigations of different angular correlations between the final state particles. As an example, we calculated the distributions on the angle θ between the produced Z boson and b-quark in the Collins–Soper frame (where the z axis is defined with respect to the bisector of colliding protons in the $b\bar{b}$ rest frame), and on the azimuthal angle difference $\Delta\phi$ between the final beauty quarks in the pp center-of-mass frame. The results of our calculations performed near the Higgs boson peak (with $120 < M < 130$ GeV) are shown in Figs. 5 and 6, where an additional cut $p_T > 200(300)$ GeV is applied at $\sqrt{s} = 8(14)$ TeV. As expected, the isotropic decay of the scalar Higgs particle $H \to b\bar{b}$ greatly differs from the angu-

lar distributions predicted by the off-shell amplitudes of the subprocesses (2) and (3). Moreover, the beauty quarks, originating from the Higgs boson decay, populate mostly low $\Delta\phi$ (see Fig. 6), whereas the leading QCD background, as given by the gluon–gluon fusion subprocess (3), has a flatter $\Delta\phi$ distribution. So, the different angular correlations between the final state particles in the associated $Zb\bar{b}$ production are very sensitive to the source of the $b\bar{b}$ pairs, and therefore future experimental investigations of such observables at the LHC with increased luminosity can give clear information as regards the Higgs signal.

Finally, we study the size of the theoretical uncertainties of our calculations connected with the hard scale. As usual, in order to estimate these uncertainties we vary the scales by a factor of 2 around their default values. Also, we use the CCFM set A0+ and A0− instead of the default TMD gluon density A0. These two PDF sets represent a variation of the hard scale involved in (18) and (19). The A0+ stands for a variation of 2μ, while set A0− reflects $\mu/2$. We observe a deviation of about 50 % with both A0+ and A0− sets (see Fig. 7) for the QCD background (as given by the sum of gluon–gluon fusion and quark–antiquark annihilation subprocesses considered above). Despite the relatively large band of uncertainties, this does not change our conclusions. Additionally, to investigate the role of higher-order QCD corrections, in Fig. 7 we present the results for the QCD background obtained in the framework of collinear QCD factorization at LO. We find that in the kinematical region where the possible Higgs signal could be observed these corrections are important.

To conclude, in the present note we applied the k_T-factorization approach of QCD to study the possibility to detect the scalar Higgs boson decay $H \to b\bar{b}$ in the associated Z and $b\bar{b}$ production at the LHC. Our considera-

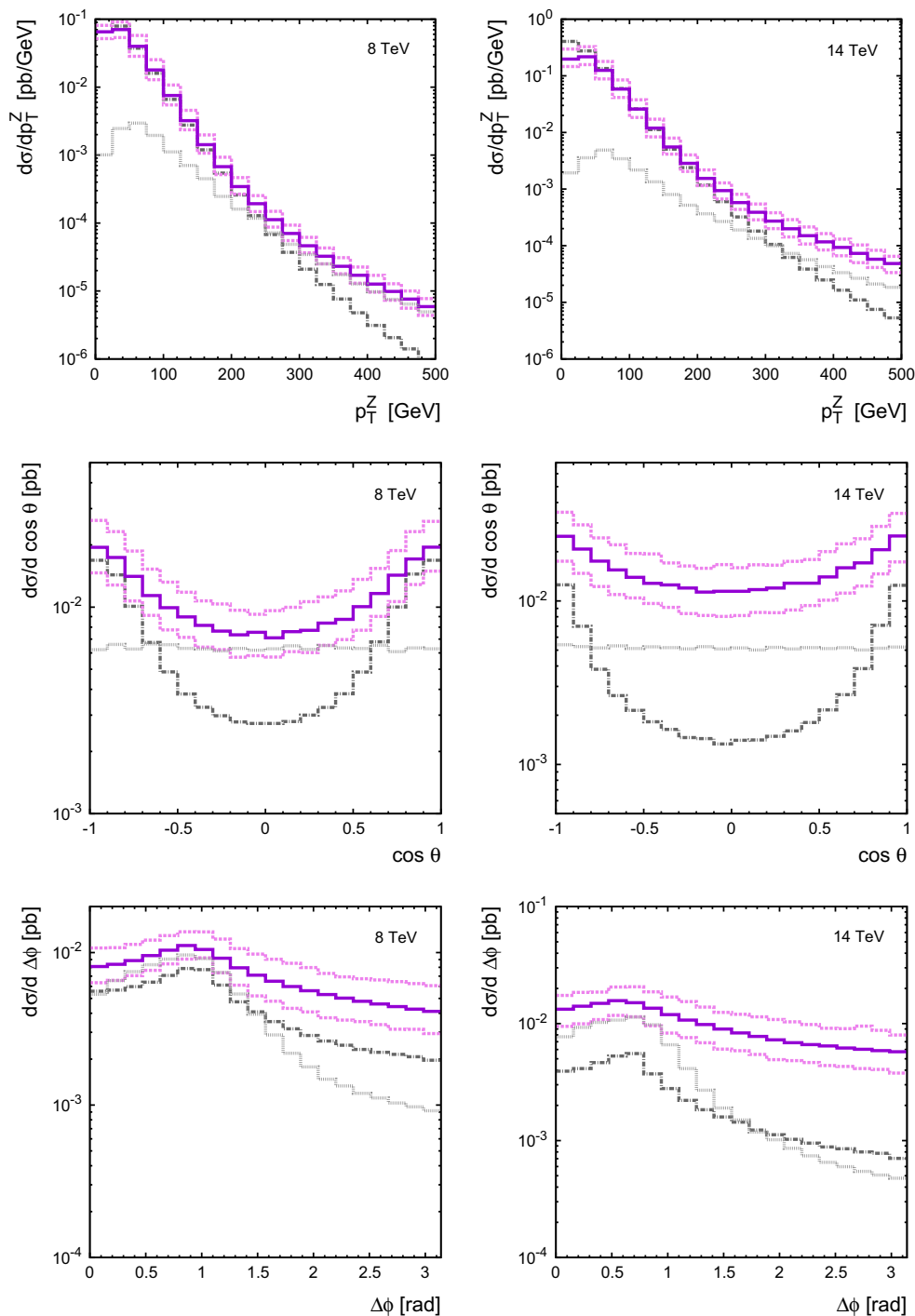**Fig. 7** The associated $Z + b\bar{b}$ cross sections in pp collisions calculated as a function of Z boson transverse momentum p_T, angle θ, and azimuthal angle difference $\Delta\phi$ at $\sqrt{s} = 8$ TeV (*left panel*) and $\sqrt{s} = 14$ TeV (*right panel*) at $120 < M < 130$ GeV. The *solid* and *dash-dotted histograms* correspond to the QCD background (sum of the gluon–gluon fusion and quark–antiquark annihilation subprocesses) calculated in the framework of the k_T-factorization approach and collinear approximation of QCD at LO, respectively. The *upper* and *lower dashed histograms* correspond to the scale variations in the k_T-factorization predictions, as described in the text. The *dotted histograms* correspond to the contributions from the $q^*\bar{q}^* \to ZH \to Zb\bar{b}$ subprocess. An additional cut $p_T > 200(300)$ GeV is applied for $\sqrt{s} = 8$ (14) TeV in the θ and $\Delta\phi$ distributions

tion was based on the off-shell production amplitudes of $q^*\bar{q}^* \to ZH \to Zq'\bar{q}'$, $q^*\bar{q}^* \to Zq'\bar{q}'$, and $g^*g^* \to Zq'\bar{q}'$ partonic subprocesses supplemented with the CCFM dynam-

ics of parton densities in a proton. The main part of the higher-order QCD corrections (corresponding to the $\log 1/x$ enhanced terms in a perturbative series) is effectively taken

into account in our consideration. We demonstrated that the $H \to b\bar{b}$ signal can be observed at large transverse momenta near the Higgs boson peak despite the overwhelming QCD background, and we pointed out the important role of the angular correlations between the produced Z boson and b-quarks. The gauge invariant off-shell amplitudes of $q^*\bar{q}^* \to ZH \to Zq'\bar{q}'$ and $q^*\bar{q}^* \to Zq'\bar{q}'$ partonic subprocesses, calculated for the first time, can be implemented in different Monte Carlo event generators, like, for example, CASCADE [53,54].

References

1. CMS Collaboration, Phys. Lett. B **716**, 30 (2012)
2. ATLAS Collaboration, Phys. Lett. B **716**, 1 (2012)
3. ATLAS Collaboration, JHEP **09**, 112 (2014)
4. M. Spira, A. Djouadi, D. Graudenz, P. Zerwas, Nucl. Phys. B **453**, 17 (1995)
5. A. Djouadi, M. Spira, P.M. Zerwas, Phys. Lett. B **264**, 440 (1991)
6. S. Dawson, Nucl. Phys. B **359**, 283 (1991)
7. R.V. Harlander, W.B. Kilgore, Phys. Rev. Lett. **88**, 201801 (2002)
8. C. Anastasiou, K. Melnikov, Nucl. Phys. B **646**, 220 (2002)
9. V. Ravindran, J. Smith, W.L. van Neerven, Nucl. Phys. B **665**, 325 (2003)
10. S. Catani, D. de Florian, M. Grazzini, P. Nason, JHEP **0307**, 028 (2003)
11. D. de Florian, G. Ferrera, M. Grazzini, D. Tommasini, JHEP **1111**, 064 (2011)
12. CMS Collaboration, Phys. Rev. D **89**, 092007 (2014)
13. CMS Collaboration, JHEP **01**, 096 (2014)
14. LHC Higgs Cross Section Working Group Collaboration, CERN-2011-002
15. CDF and D0 Collaborations, Phys. Rev. Lett. **109**, 071804 (2012)
16. CMS Collaboration, Phys. Rev. D **89**, 012003 (2014)
17. L.V. Gribov, E.M. Levin, M.G. Ryskin, Phys. Rep. **100**, 1 (1983)
18. E.M. Levin, M.G. Ryskin, YuM Shabelsky, A.G. Shuvaev, Sov. J. Nucl. Phys. **53**, 657 (1991)
19. S. Catani, M. Ciafaloni, F. Hautmann, Nucl. Phys. B **366**, 135 (1991)
20. J.C. Collins, R.K. Ellis, Nucl. Phys. B **360**, 3 (1991)
21. B. Andersson et al., Small-x Collaboration. Eur. Phys. J. C **25**, 77 (2002)
22. J. Andersen et al., Small-x Collaboration, Eur. Phys. J. C **35**, 67 (2004)
23. J. Andersen et al., Small-x Collaboration, Eur. Phys. J. C **48**, 53 (2006)
24. A.V. Lipatov, M.A. Malyshev, N.P. Zotov, Phys. Lett. B **735**, 79 (2014)
25. A. Szczurek, M. Luszczak, R. Maciula, Phys. Rev. D **90**, 094023 (2014)
26. L.N. Lipatov, M.I. Vyazovsky, Nucl. Phys. B **597**, 399 (2001)
27. A.V. Bogdan, V.S. Fadin, Nucl. Phys. B **740**, 36 (2006)
28. L.N. Lipatov, Nucl. Phys. B **452**, 369 (1995)
29. L.N. Lipatov, Phys. Rept. **286**, 131 (1997)
30. M. Hentschinski, A. Sabio Vera, Phys. Rev. D **85**, 056006 (2012)
31. M. Hentschinski, Nucl. Phys. B **859**, 129 (2012)
32. G. Chachamis, M. Hentschinski, J.D. Madrigal Martinez, Nucl. Phys. B **861**, 133 (2012)
33. S.P. Baranov, A.V. Lipatov, N.P. Zotov, Phys. Rev. D **89**, 094025 (2014)
34. V.A. Saleev, Phys. Rev. D **80**, 114016 (2009)
35. J.A.M. Vermaseren, NIKHEF-00-023 (2000)
36. S.P. Baranov, A.V. Lipatov, N.P. Zotov, Phys. Rev. D **78**, 014025 (2008)
37. M. Deak, F. Schwennsen, JHEP **0809**, 035 (2008)
38. M. Ciafaloni, Nucl. Phys. B **296**, 49 (1988)
39. S. Catani, F. Fiorani, G. Marchesini, Phys. Lett. B **234**, 339 (1990)
40. S. Catani, F. Fiorani, G. Marchesini, Nucl. Phys. B **336**, 18 (1990)
41. G. Marchesini, Nucl. Phys. B **445**, 49 (1995)
42. H. Jung, arXiv:hep-ph/0411287
43. M. Deak, H. Jung, K. Kutak, arXiv:0807.2403 [hep-ph]
44. F. Hautmann, M. Hentschinski, H. Jung, Nucl. Phys. B **865**, 54 (2012)
45. S. Catani, F. Hautmann, Nucl. Phys. B **427**, 475 (1994)
46. S. Catani, F. Hautmann, Phys. Lett. B **315**, 157 (1993)
47. G. Curci, W. Furmanski, R. Petronzio, Nucl. Phys. B **175**, 27 (1980)
48. F. Hautmann, M. Hentschinski, H. Jung, arXiv:1207.6420 [hep-ph]
49. A.D. Martin, M.G. Ryskin, G. Watt, Phys. Rev. D **70**, 014012 (2004)
50. A.D. Martin, M.G. Ryskin, G. Watt, Eur. Phys. J. C **31**, 73 (2003)
51. A. Kulesza, W.J. Stirling, Nucl. Phys. B **555**, 279 (1999)
52. G.P. Lepage, J. Comput. Phys. **27**, 192 (1978)
53. H. Jung, G.P. Salam, Eur. Phys. J. C **19**, 351 (2001)
54. H. Jung et al., Eur. Phys. J. C **70**, 1237 (2010)